Thermal characteristics of permafrost in the steep alpine rock walls of the Aiguille du Midi (Mont Blanc Massif, 3842 m a.s.l)

F. Magnin[1], P. Deline[1], L. Ravanel[1], J. Noetzli[2], P. Pogliotti[3]

[1]{EDYTEM Lab, Université de Savoie, CNRS, Le Bourget-du-Lac, France}

[2]{Glaciology and Geomorphodynamics Group, Department of Geography, University of Zurich, Zurich, Switzerland}

[3]{ARPA Valle d'Aosta, Saint-Christophe, Italy}

Correspondence to:

F. Magnin (florence.magnin@univ-savoie.fr)

P. Deline (philip.deline@univ-savoie.fr)

L. Ravanel (ludovic.ravanel@univ-savoie.fr)

J. Noetzli (jeannette.noetzli@geo.uzh.ch)

P. Pogliotti (paolo.pogliotti@gmail.com)

Abstract

Permafrost and related thermo-hydro-mechanical processes are regarded as probable factors in high alpine rock wall stability, but a lack of field measurements means that the characteristics and processes of rock wall permafrost are poorly understood. To help remedy this situation, in 2005 work began to install a monitoring system at the Aiguille du Midi (3842 m a.s.l). This paper presents temperature records from nine surface sensors (eight years of records) and three 10-m-deep boreholes (four years of records), installed at locations with different surface and bedrock characteristics. Analysis of the temperature data confirm previous studies, some of them being demonstrated empirically for the first time: micro-meteorology controls the surface temperature, active layer thicknesses are directly related to aspect and ranged from <2 m to nearly 6 m, warm and cold permafrost (about –1.5°C to –4.5°C at 10-m-depth) coexists within the Aiguille du Midi, resulting in high lateral heat fluxes, thin accumulations of snow and open fractures are cooling factors. Some observations extent existing knowledge: thick snow accumulations warm north faces but cool south faces, possibly inhibit active layer refreezing in winter and delay its thawing in summer. Latent heat consumption due to interstitial water phase changes in bedrock discontinuities possibly dampens the active layer and permafrost changes, whereas an open fractures act as a thermal cutoff in the sub-surface thermal regime. Our field data, the first to be obtained from an Alpine permafrost site where borehole temperatures are below –4°C, are promising for developing strategies of investigation of poorly known factors in steep bedrock permafrost such as the effect of snow cover and fracturing.

1 Introduction

The last few decades have seen an increase in rockfall activity from steep, high-altitude rock walls in the Mont Blanc Massif (Western European Alps) (Ravanel and Deline, 2010; Deline et al., 2012). Several studies of recent rock avalanches and rockfalls in mid-latitude alpine ranges have ascribed such increases to climate-related permafrost degradation (Deline, 2001; Gruber et al., 2004a; Huggel et al., 2005; Fischer et al., 2006; Huggel et al., 2008; Allen et al., 2009; Ravanel et al., 2010, 2012; Deline et al., 2011). Rockfall magnitude and frequency are thought to be linked to the timing and depth of permafrost degradation, which can range from a seasonal deepening of the active layer to long-term, deep-seated warming in response to a climate signal (Gruber and Haeberli, 2007). Local warming of cold permafrost may be induced by advection and the related erosion of cleft ice (Hasler et al., 2011b), which may lead to unexpected bedrock failures. As Krautblatter et al. (2011) noted, before being able to predict permafrost-related hazards, it is first necessary to develop a better understanding of the thermo-hydro-mechanical processes involved, which means collecting rock temperature measurements and develop modeling strategies.

Measurement strategies and numerical experiments have been used to investigate the thermal conditions and characteristics of near-vertical and virtually snow-free alpine rock walls that are directly coupled with the atmosphere (Gruber et al., 2003; 2004b, Noetzli et al., 2007). These studies have shown the domination of topography control on steep bedrock permafrost distribution, with a typical surface temperature difference of 7-8°C between south and north faces, the possible coexistence of warm and cold permafrost in a single rock mass and lateral heat fluxes within the rock mass inducing near-vertical isotherms. Hasler et al. (2011a) suggested that, compared with snow-free, smooth rock faces, thin accumulations of snow on micro-reliefs and cleft ventilation may both cause deviations of 1°C (shaded faces) to 3°C (sun-exposed faces) compared with the smooth, snow-free rock wall model test case. The thermal influence of snow on steep rock faces has been specifically addressed with numerical experiments (Pogliotti, 2011), showing the high variability of its effect depending on topography, depth and timing of the accumulation, but empirical evidences in such a context are still scarce. These recent advances in the study of steep, alpine rock walls have helped to build bridges between what is known about the general characteristics of permafrost and processes related to the microtopography and internal structure of the rock mass, which may be significant in the short-term evolution and in permafrost distribution. However, a much larger corpus of field observations and monitoring data for a variety of bedrock conditions is needed to develop, calibrate, and evaluate reliable models.

As part of our research into geomorphic activity in the Mont Blanc Massif, in 2005 we started a long-term permafrost-monitoring program at the Aiguille du Midi (AdM), that is presently the highest instrumented bedrock permafrost site in the European Alps (3842 m a.s.l). This monitoring program was designed to meet three scientific goals:

The monitoring program was designed to meet three scientific goals:

1. characterize the surface temperatures of high-alpine steep rock walls;
2. determine the thermal state of permafrost and analyze the variability of active-layer and deep temperature;

3. collect temperature data under variable snow-cover and structural conditions useful for calibrating and validating high-resolution numerical experiments on permafrost thermal processes.

The present paper addresses goals (i) and (ii). It describes the monitoring program at the AdM, presenting temperature data from nine surface mini-loggers and three 10metersdeep boreholes. Due to the peak morphology of the AdM, the monitoring network is concentrated in a very small area. The sensors are installed in order to investigate differing snow cover conditions and bedrock structure. Such a network design allows to address the following research questions:

- How much is the surface temperature variability due to topography in a so small area?

- How much can be the thermal effect of snow cover on surface temperature in steep rockwalls?

- How much is the variability of active layer due to topography in steep rockwalls?

- What are the thermal effects of snow and fractures on sub-surface temperatures at the AdM?

We analyze seasonal and annual patterns of surface temperature, active layer and permafrost thermal regime from eight years of surface records and four years of borehole data discussing our results at the light of former studies and providing new empirical evidences of the poorly known effect of snow and fractures on permafrost in steep rock walls.

2 Study site

Located on the NW side of the Mont Blanc massif (Fig. 1), the summit of the AdM (45.88° N, 6.89°E) consists of three granite peaks (Piton Nord, Piton Central, and Piton Sud) and culminates at 3842 m a.s.l. The steep and partly glaciated north and west faces of the AdM tower more than 1000 m above the Glacier des Pélerins and Glacier des Bossons, while its south face rises just 250 m above the Glacier du Géant (i.e., the accumulation zone of the Mer de Glace). This part of the Mont Blanc Massif is formed by an inclusion-rich, porphyritic granite and is bounded by a wide shear zone. A main, N 40°E fault network intersected by a secondary network determines the distribution of the main granite spurs and gullies (Leloup et al., 2005). The highest parts of the peak tend to be steep, contain few large fractures, and, in places, are characterized by vertical foliation bands and small fissures. The lower parts are less steep and more fractured. In the present paper we use the abbreviation AdM to refer only to the upper section of the Piton Central, between 3740 and 3842 m a.s.l. where most of the instruments are installed. A tourist cable car runs from Chamonix to the Piton Nord. Galleries and an elevator allow visitors to gain the viewing platform on top of the Piton Central, from where there is a 360° panorama of the Mont Blanc Massif.

We chose the AdM as a monitoring site for the following scientific and logistical reasons: (i) permafrost is extremely likely due to the AdM's high altitude and the presence of cold-based hanging glaciers on its north face; (ii) the morphology of the peak, which offers a range of aspects, slope angles, and fracture densities that are representative of many other rock walls in the massif; (iii) the easy access by cable-car from Chamonix and the availability of services (e.g., electricity) at the summit station. Monitoring equipment was installed as part of the *PERMAdataROC* (2006–2008) and *PermaNET* (2008–2011) projects, funded by the European Union and run jointly by EDYTEM Lab (France), ARPA VdA (Italy), and the Universities of Zurich (Switzerland), Bonn, and Munich (Germany). As such it complements other rock wall observation sites, for example, those within the Swiss Permafrost Monitoring Network (PERMOS).

In complement to the monitoring equipment, weather stations from the ARPA VdA which measured air temperature and relative humidity, incoming and outgoing shortwave and longwave solar radiation, wind speed, and wind direction on the south and north faces worked from 2006 to 2010. Electrical Resistivity Tomography (ERT) and Induced Polarization (IP) are measured since 2008 with the Universities of Bonn and Munich. High-resolution (cm-scale) triangulated irregular networks (TIN) of rock walls and galleries of the AdM were obtained from terrestrial laser scanning. Six crack-meters equipped with a wireless sensor network were installed in July 2012 at major fractures of the Piton Central and Piton Nord to complete existing studies of cleft dilatations and shearing movements in rock wall permafrost, to check the AdM stability and to test an early warning system. Finally, two GPR surveys were performed along vertical transects since 2013. All these data are not used for this study but will support our project.

3 Data collection methods

3.1 Rock temperature monitoring

The present study uses rock surface temperatures at the top of the AdM (between 3815 and 3825 m a.s.l.; Fig. 2) that is monitored since 2005 using mini-loggers (GeoPrecision PT1000 sensors, accuracy ±0.1°C) and was installed by the University of Zurich and ARPA VdA. Each face of the AdM has two loggers installed in snow free locations (Table 1). The south face has an additional logger (S3) installed just above a small ledge on which snow accumulates in winter, covering the logger. The loggers record the temperature every hour at depths of 0.03, 0.30, and 0.55 m, in line with the method described by Gruber et al. (2003).

In September 2009, three boreholes were drilled in the lower section of the Piton Central, at between 3738 and 3753 m a.s.l.

In order to minimize possible thermal disturbances, the boreholes were drilled several tens of meters below the galleries running through the AdM. The possible disturbances in the Piton Central are assumed to be related to air ventilation and heating from the local workers team rooms especially, but because of the pluri-decametric vertical distance in between the galleries and the boreholes, we assume that these last ones are not affected by the anthropogenic disturbance. The exact location of each borehole was chosen according to the aspect, fracturing, roughness, and angle of the rock wall (Fig. 2). Each borehole was drilled perpendicular to the rock surface and to a depth of 11 meters. Borehole depths were constrained by the drilling equipment and the funding available. The boreholes on the northeast (BH_E) and south (BH_S) faces were drilled in fractured rock walls that slope at 65° and 55°, respectively. Even on rock walls at these angles, snow can accumulate on the micro-reliefs in the face. The borehole on the northwest face (BH_N) was drilled in a vertical, unfractured wall. The only place that snow can accumulate on this wall is on small ledges such as the one above which BH_N was drilled.

The boreholes were drilled between September 14th and September 27th, 2009 by a team of five people (two mountain guides, plus three members of the EDYTEM Lab) who had to contend with very variable weather and challenging logistics. For each borehole it was necessary to: (i) install a safety line for the workers, (ii) set up a rope system to carry the equipment from the galleries to the drill site, (iii) install a work platform for the three drillers, (iv) anchor a base on which to fix a rack way, (v) drill the hole using a 380-V Weka Diamond-Core DK 22 electric drill, (vi) insert into the hole a polyethylene PE100 tube (outer diameter: 40 mm; inner diameter: 29 mm) sealed at its bottom, and (vii) remove the work platform. In addition to the difficult environment and harsh weather, the drilling work was complicated by the heterogeneity and hardness of the granite, which took a heavy toll on the equipment (11 diamond heads worn out or broken, a dozen steel tubes damaged, and a motor broken). At first we tried to drill 46-mm-diameter boreholes but we had to increase the diameter to 66 mm so we could use a more robust pipe string. Cooling required 1 to 3 m^3 of water per day, which was carried up from Chamonix in 1-m^3-tanks via the cable car. Space between the drilling hole and the casing tube has not been filled.

The three boreholes were fitted with Stump 10-m-long thermistor chains, each with 15-nodes (YSI 44031 sensors, accuracy ±0.1°C) arranged along a 6-mm fiberglass rod. Following calibration at 0°C in an ice-water basin, the sensors were inserted in BH_S and BH_N in December 2009 and in BH_E in April 2010 (Fig. 3). In order to prevent heat convection, each sensor was separated from the others on the chain by insulating foam. The boreholes were closed at the top, but the chains can be removed to check for thermistor drift. Rock temperatures at depths between 0.3 and 10 m are recorded every three hours (Table 1). Because BH_S is shallower than 10 m, the thermistor chain protrudes from the rock surface by 36 cm. Temperature comparisons between BH_S and BH_N/BH_E were carried out at the closest equivalent depths (*e.g.*, temperatures at a depth of 2.64 m in BH_S were compared with temperatures at a depth of 2.5 m in BH_E and BH_N).

3.2 Air temperature and snow cover measurements

To support the analysis of rock temperature, we use air temperature that is monitored by Météo France since 2007 at a station located 3 m above the top of the Piton Central (3845 m a.s.l.) Data prior to 2007 (1989–2006) are very fragmented due to insufficient equipment maintenance and are not used in this study in which we only use air temperature time series (AT, Table 1).

In January 2012, two automatic cameras taking six pictures per day of the south and northeast borehole sites have been installed. In addition, five graduated stakes have been placed in the surroundings of each borehole to evaluate the spatial variability of snow accumulation on pictures. The visual analysis of pictures of winters 2012 and 2013 reveals a spatially homogeneous thick snow cover (>1m) lasting until late spring on BH_S and a thin (<0.5 m) spatially variable snow cover on the BH_E due to the higher steepness and complex geometry of the rock mass These observations are reported in Table 1. Snow accumulation over BH_N and S3 is estimated from field observations. At BH_N, snow accumulation is restricted to the relatively large ledge above which the borehole is drilled and the snow patch is over 1 m thick for most of the year. S3 is also frequently covered by > 0.5 m of snow accumulating during winter and spring on the small ledge above which the sensor is installed. But snow depth is more variable on S3 than on BH_N because of the intense solar radiation that leads to more frequent melting.

4 Dataset preparation

The borehole time series are all continuous except for short periods for BH_S, as this logger was removed from September 2012 to January 2013 and from October 2013 to January 2014 to prevent it being damaged by engineering work close to the borehole. Gaps in the 0.3 m temperature and AT time series were filled in so we could calculate seasonal and annual means (cf. Table 2). First, daily means from rock temperature time series were calculated for complete days of records. Then, short gaps (< 5 days) were filled by linear interpolation between the nearest available data points for the same depth; longer gaps (up to 1.5 month) were filled by replacing missing data with the average value for the 30 days before and 30 days after the gap (cf. Hasler et al., 2011a). To fill the longest gaps for E1, N1, S1, and W1 (from December 4th, 2007 to February 7th, 2008) we used a third approach that involved applying a linear regression equation, fitted using data from each pair of loggers (e.g., E2 and E1) and from the gap periods (*i.e.*, December-February) for groups of years with complete records (2006–2007 and 2008–2009). Correlation coefficients for the equations ranged from 0.89 (S1 and S2) to 0.94 (E1 and E2). We tested this approach by simulating corresponding gap periods in the years with complete data and then filling these gaps using the regression equations. Differences between the annual means obtained using this method and the annual means calculated from the complete data set were in the range 0.01-0.15°C and can be considered negligible. Our calculations of seasonal means did not include data obtained using the 30-day average or linear regression methods. We did not fill gaps longer than 1.5 month per year because we felt that the resulting data would not be reliable enough to give realistic annual means.

5 Rock surface temperature

Smith and Riseborough (2002) defined Surface Offset (SO) as the difference between local Mean Annual Air Temperature (MAAT) and Mean Annual Ground Surface Temperature (MAGST). Surface offset is a parameter in the TTOP model (Temperature at the Top of Permafrost, Smith and Riseborough, 1996), originally developed to define the functional relation between air and ground temperatures in polar lowlands and later applied to high-latitude mountainous terrain (Juliussen and Humlum, 2007). SO can be used to quantify the overall effect of ground cover and ground surface parameters on the surface energy balance.

We calculated both annual SOs (ASO), using annual means, and seasonal SOs (SSO) using seasonal means of rock surface and air temperature of the season for winter (December to February), spring (from March to May), summer (from June to August), and fall (from September to November), using time series measured at depths of 0.3-m (boreholes and E2, S2, W2, N2) and 0.1-m (E1, S1, W1, N1) - points we considered representative of surface conditions. We applied a standard lapse rate of 0.006°C.m^{-1} on air temperature in order to balance the elevation difference between the Météo France station and the sensors. Figure 4 shows ASOs for all the complete years (Fig. 4A), SSOs for snow-free sensors for the available seasons (Fig. 4B), and SSOs for snow-covered sensors for the available seasons (Fig. 4C). The SO description are then completed with the analysis of the daily temperature of snow-covered sensors and air temperature trend (Fig. 5) to support the discussion on the snow control on surface temperature.

5.1 Surface Offset patterns

Spatially, maximum and minimum ASOs were 9.3°C, recorded at S1 in 2011, and 1.3°C, recorded at N1 in 2009 (Fig. 4A), which are typical values for the Alps (PERMOS, 2013). On the south face, the snow-covered sensors gave lower values than the snow-free sensors. For example, the ASOs for S3 were between 0.1°C (2010) and 1.4°C (2011) lower than the ASOs for S1. Conversely, on the north side, the snow-covered sensor gave higher ASOs than the snow-free sensors. At the seasonal scale, the maximum SSOs occurred in summer for the snow-free sensors (Fig. 4B), except for the sensors on the south face (S1 and S2), where the maximum SSOs occurred in spring, with values >10°C. The lowest SSOs were recorded in winter, and ranged from approximately 8°C on the south face to <1°C on the north face (N1 and N2). SSO patterns for the snow-covered sensors (Fig. 4C) were opposite to those for the snow-free sensors, except for BH_E. At BH_N and BH_S, SSOs were largest in winter (4.1°C and 9.5°C, respectively) and lowest in summer. At S3, autumn SSO was the largest, and it was also relatively high for BH_N and BH_S. Unlike the other snow-covered sensors, SSOs at BH_E remain coherent with insolation duration, similarly to snow free sensors.

Temporally, snow-covered and shaded sensors such as BH_E and BH_N show high interannual variability between 2011 and 2012 (+1.1°C), that is not visible at snow-free sensors, and at snow covered and south-facing sensors (only +0.3°C at S3). Conversely to the snow-covered sensors, the 2011-2012 ASO decreased at the snow-free sensors, with, for example, values of -1°C at S2 and -0.3°C at E1. The maximum and minimum ASOs for the different snow-free sensors did not occur in the same years. Even though both sensors of a similar aspect (e.g. N1 and N2) showed similar interannual changes, these changes were not consistent from one aspect to another, with, for example, the maximum ASOs at W1 and W2 in 2008, but in 2011 at S1 and S2.

5.2 Daily temperature of snow covered sensor

At the daily scale, temperature curves of the snow covered sensors are smoothed compared to air temperature oscillation during the cold period (Fig. 5). The S3 and BH_S temperature curves were strongly smoothed from mid-November 2010 to January (BH_S) or April 2011 (gap for S3), and from early December 2011 to mid-May 2012. Both sensors recorded a period of almost 0°C isothermal conditions from April to mid-May 2012. The temperature curve for BH_N was strongly smoothed until the summer, with a similar 0°C isothermal period during three weeks in July 2011. Although the BH_E temperature curve from late September to February-March was mostly smoother than the air temperature daily oscillations, both curves were more closely coupled than for the other sensors, as BH_E oscillated in-synch with major changes in AT, such as the large drop in temperature in December 2012. The temperatures recorded at BH_E were lower than those recorded at BH_N during certain periods (September 2010 to March 2011, November 2011 to February 2012).

5.3 Snow cover and micro-meteorology influences

Normally on steep, snow-free bedrock in high mountain, the MAGST is higher than MAAT. Such a difference is mainly due to direct solar radiation (Gruber et al. 2004b) and partly due to reflected solar radiation from large, bright glacier surfaces below the measurement points (PERMOS, 2013). In the European Alps, the ASO can be up to 10°C on south-facing rock walls. In Norway, maximum ASO values recorded on steep rock walls are only 3°C, as there is less direct solar radiation at the higher latitudes (Hipp et al., 2014). In New Zealand, thus at a similar latitude of the Alps, Allen et al. (2009) reported a maximum ASO value of 6.7°C. Such a lower value can be ascribed to a reduction of direct solar radiation due to the influence of the oceanic climate and related frequent cloud cover. In these studies most of the surface sensors have been installed in snow-free conditions with the purpose of testing energy balance models (Gruber et al., 2004b) or for statistical fitting (Allen et al., 2009, Boeckli et al., 2012). At the AdM patterns of snow-covered sensors are different from snow-free sensors, mainly due to the decoupling from the atmospheric conditions during the winter season and reduction of surface albedo.

The differences in ASOs between snow covered and snow free sensors on similar aspect demonstrate that snow exerts a significant control on the annual energy balance. According to empirical and numerical studies (Hanson and Hoelzle, 2004; Luetschg et al., 2008), a snow thickness > 0.6-0.8 m insulates the rock surface from air temperature, but in steep rock walls, snow cover is usually thinner than this insulating threshold (Gruber and Haeberli, 2009). The differences between BH_N and BH_E in terms of ASOs and SSOs can be probably ascribed to variations of mean snow cover thickness (Table 1), and demonstrate that the insulating effect of snow can occur locally also in steep rock walls. On the north face, the higher ASOs at snow-covered sensors (BH_N) compared to at snow-free sensors (N1 and N2) show that the thermo-insulation of snow significantly increases the MAGST. On the south face, the lower ASOs at snow covered sensors (BH_S and S3) compared to snow free conditions (S1 and S2) indicates a lowering of MAGST due to snow. This cooling effect results from the combination of (i) a thin snow cover with negligible thermo-insulation, (ii) an increase of surface albedo, (iii) and melt energy consumption (Harris and Corte, 1992; Pogliotti, 2011). At the AdM, the latter two factors seems to be prevalent since the snow cover thickness on south face is proved to be often > 1 m during winter (sect 3.2) with appreciable smoothing of daily temperature oscillations (Fig. 5).This observation extents previous study on thin snow accumulations (Hasler et al. 2011a). The importance of this cooling effect on sunny faces is likely reinforced by the long lasting of the snow over the year at such elevation, as suggested by (i) the high autumn SSOs (early snow accumulation) for snow covered sensors, (ii) their low summer SSO, and (iii) by the nearly-isothermal conditions at 0°C occurring in late summer (Fig. 5) and probably reflecting the zero-curtain effect (e.g. Hanson and Hoelzle, 2004; Gubler et al., 2011).

The inter-annual variability of ASO is not spatially homogeneous. Snow-covered and snow-free sensors exhibit different behavior, thereby complementing the PERMOS reports (2013), which showed differences in interannual variability between rock walls and gentle snow-covered terrain. The interannual variability of snow-free sensors is mainly related to differences in insolation due to clouds, and the differences within this interannual variability from on aspect to another can be interpreted as a difference in cloud formation from year-to-year. The difference in the spatial distribution of MAGST over a same rock peak due to the effect of convective cloud formations was already shown by energy balance models (Noetzli et al., 2007), but the evolution of these differences through time with the micro-meteorological control was poorly explored. On shaded faces, the solar radiation control is largely reduced and snow may have more influence on the interannual changes. Consequently, the temperature at a snow-covered sensor can increase from one year to the next if the snow insulation from the atmospheric temperature increases meanwhile the temperature at a snow-free sensor may drop due to reduced insolation. In the case of sun-exposed and snow covered sensor, such as S3, the balance between the warming and the cooling effects leads to smaller interannual ASO variability than at sensors in shadier locations mostly controlled by the warming effect of snow insulation. Thus, the snow influence on the surface temperature of high-elevated rock walls is a result of the combination between the topography, snow depth and micro-meteorology.

6 Borehole records

Four years of data from the three boreholes allowed us to describe the patterns of daily temperature (Fig. 6), mean annual Temperature-Depth (T(z)) profiles, and annual temperature envelopes (*i.e.*, the maximum and minimum daily temperatures at each depth in 2011; Fig. 7). We focused on the active layer and the permafrost thermal regime, paying special attention to thermal effects related to snow cover and bedrock structure which possible influence on the active layer and bedrock thermal regime is discussed in the light of present knowledge.

6.1 Active layer

Active Layer Thickness (ALT) varied with aspect, with means of ca. 3 m at BH_E, 5.5 m at BH_S, and 2.2 m at BH_N (Fig. 6). Interannual variability during the monitoring period was ca. 0.7 m for each borehole (Table 3). The maximum ALT for each borehole occurred in 2012 for BH_N (2.5 m deep), in 2013 for BH_E (3.4 m deep), and in 2011 for BH_S (5.9 m deep; however, there are no relevant data for 2012).

The length of the thawing period, marked by continuous positive temperatures at the uppermost thermistor, also varies according to aspect. It is longest at BH_S, starting in June (April in 2011), but with isolated thawing days already in March (e.g., in 2012). In general, BH_S surface refroze in October but total refreezing of the active layer did not occur until December in 2010 and 2011. The 2011–2012 freezing period was particularly mild and short (3–4 months) at BH_S. This pattern was not as marked at BH_E, which even recorded its lowest surface temperature in 2011–2012. BH_N had the longest freezing periods because temperatures in the rock sub-surface remained positive only from June to October. In 2011, thawing did not start until August. BH_E had the most balanced thawing and freezing periods (ca. 6 months each).

The timing of maximum ALT depended on aspect and year (Table 3). In 2010 and 2011, maximum ALT occurred earliest at BH_E, even though the active layer was thicker at BH_E than at BH_N. In 2012 and 2013, BH_N was the first site to reach maximum ALT. In 2010, maximum ALT at BH_S occurred very late, three months later than at BH_E. Although the BH_S active layer had mostly thawed by mid-July, thawing continued steadily until the end of October. Maximum ALT always occurred later at BH_S than at the other boreholes, but the lowering of the 0°C isotherm was more linear.

6.2 Thermal regime

Annual Temperature-Depth T(z) profiles (Fig. 7A) revealed different thermal regimes. The AdM's Piton Central has both warm (ca. –1.5°C at BH_S) and cold (ca. –4.5°C at BH_N) permafrost (Table 3). Interannual changes were not similar in every borehole. In BH_N and BH_E the changes along the 2010-2013 period generally followed the changes in MAAT all along the T(z) profiles (Table 3), except for 2011 in BH_N that is significantly warmer than other years from the surface to 2.5 m-depth and is colder than 2012 from 3 m-depth and than

2013 from 7 m-depth. In BH_S, the mean annual T(z) profile of 2011 remarkably warms near the surface with positive temperatures to a depth of 1 m and is warmer than 2010 along the shallowest 6 m whereas it is slightly colder below.

The zero annual amplitude depth is >10 m for every borehole (Fig. 7B), which is consistent with other bedrock sites in the European Alps (PERMOS, 2007). In 2011, the largest amplitudes in daily temperature (peak to peak) at the surface (>20°C) and at 10 m depth (1.6°C) were at BH_E, and the smallest surface (15.5°C) and 10-m (1.0°C) amplitudes were at BH_N and BH_S respectively. In line with the surface pattern, the minimum T(z) profile from the surface to 1.4 m deep was warmer at BH_N than at the sunnier BH_E (Fig. 7B).

The minimum and mean annual T(z) profiles for BH_N contain two distinct sections separated by an inflection at ca. 2.5 m deep (Fig. 7A). This coincides with an 8–10 cm-wide cleft encountered at this depth during the drilling operation. The temperature gradient is negative (–0.39°C m^{-1}) from the surface to the cleft, and then positive from the cleft to 10-m-deep (from 0.16°C m^{-1} to nearly isothermal). The mean annual profiles for BH_E are almost linear and have a temperature gradient of ca. –0.2°C m^{-1}. Small inflections in the profiles (e.g., at 1.1 m, 2.5 m, and 7 m depth) occur every year. In the case of BH_S, the upper parts of the annual T(z) profiles for 2010 and 2011 differ greatly, with an almost linear temperature gradient of –0.07°C m^{-1} in 2010, and a much steeper overall temperature gradient of -2.26°C m^{-1} in 2011.

6.3 Snow cover and bedrock discontinuity controls

The coexistence of warm and cold permafrost and the opposite temperature gradients between BH_S and BH_N, that likely result from lateral heat fluxes, is in accordance with previous statements deriving from numerical simulations (Noetzli et al. 2007).

In terms of permafrost thermal regime, the BH_N shows deep temperatures colder than -4°C that is a value typical of high latitude monitoring sites such as in Svalbard (Noetzli et al., 2014a) or the warmest boreholes of the continuous permafrost zone in Alaska (Romanovsky et al., 2014).

The spatial and temporal variability of ALT is consistent with values reported for Swiss boreholes in bedrock (PERMOS, 2013). For instance, thickness and timing of the ALT in BH_E are similar to those reported at the Matterhorn-Hörnligrat site (3295 m a.s.l, vertical borehole on a crest), with values ranging from 2.89 to 3.66 m between 2008 and 2010, and maximum depth occurrence from early September to early October. In bedrock slopes, active layer thickness changes seem strongly controlled by summer air temperature. During the hot summer of 2003 for instance, the ALT at Schilthorn (2909 m a.s.l) has been deepened by twice, from 4-5 m to > 8 m depht while on debris-covered slopes such as Les Gentianes moraine or the Arolla scree slopes, located in the same area and at similar elevations, any specific thickening has been observed (PERMOS, 2013).

The different patterns of ALT variability observed at the AdM between the three boreholes (Table 3), suggest that the air temperature is not the only controlling factor. The thinning of BH_E active layer in 2011 in contrast with other two boreholes may be ascribed to the cooling effect of a summer snow fall, but the cameras and snow probes were not installed yet (sect. 3.2) to check this hypothesis. However, a significant drop in daily SO at BH_E occurred just after three precipitation episodes (in August, the 26th, and in September, the 3rd-4th and 16th-19th), which supports this hypothesis but is hardly visible on a plot. These events occurred just before BH_N maximum ALT in 2011 (Table 3). Daily SO generally decreased at BH_S just after the precipitation events, and then, rapidly increased. The snow fall would have rapidly melted and shortened its cooling effect compared to the more shaded BH_E. BH_N rather showed a general increase of its daily SO, which possibly reflects a thermo-insulating effect.

The relatively mild and short 2011–2012 freezing period at BH_S may result of snow insulation, as is suggested by the subsequent period of isothermal conditions from the surface to a depth of 3-m, which may reflect the zero-curtain effect (see sections 5.2 and 5.3). As reported by Hoelzle et al., 1999, a thick long lasting snow cover reduces both the active layer freezing by insulating from cold temperature and the active layer thawing by late snow melting. Such an effect on the active layer freeze and thaw cycles is known from studies on gentle morphologies and is poorly known in steep bedrock permafrost (Gruber et al. 2004a). A clear effect of snow insulation is visible comparing temperature variations of BH_E and BH_N (Fig. 5). In particular the winter surface temperature in BH_N are always warmer and smoothed than those in BH_E (Fig. 5) and in depth (Fig. 7B), such a warming effect of snow seems to propagate until 1.4 m. In terms of ALT, the tendency to thickening in BH_E compared to BH_N and BH_S (Table 3) may be explained by the effect of a long-lasting snow cover on the latter two boreholes.

The interannual variability of ALT is usually greater on sun-exposed faces as they respond as much to the change in air temperature as in solar radiation (Gruber et al. 2004a). However, BH_S shows similar changes than the more shaded BH_E and BH_N. Field observations during drilling have revealed the presence of wet-detritic materials in the fractures of this face which suggests latent heat consumption interstitial water and/or ice during phase-change that may explain this incoherence. Moreover, the active layer of BH_S shows late refreezing, especially in its deepest layers that can refreeze a few months after the surface (sect. 6.2, Fig. 6), which is also coherent with latent heat effects. This assumption is supported by previous studies explaining the delaying and dampening effect of latent heat consumption on the thermal response of bedrock permafrost (Kukkonen et Safanda, 2001; Wegmann et al. 1998, Noetzli et al. 2007). BH_S patterns would demonstrate that this process may also be visible at short-time scale in steep rock walls. The cooling from 2010 to 2011 of its mean annual T(z) profile from 6 to 10-m-depth which is inconsistent with the MAAT change (Fig. 7, Table 3) also supports this assumption as this likely results of a dampened and delayed response. The probable control of latent heat in BH_S is reinforced by its temperature range which allows for phase-change processes. The snow accumulation and melting on the south face constitute an obvious source of water supply to fill bedrock discontinuities.

Such possible latent heat controls are not visible at BH_E and BH_N, which interannual changes are coherent with MAAT changes up to 10-m-depth, except for BH_N in 2011 (Fig. 7A). The significant warming above the cold inflection is in coherence with MAAT change from 2010 to 2011, but the colder conditions below the inflection has no coherence with climatic signal. The fracture seems to act as a thermal cutoff between the surface layer and the deep bedrock. The sharp inflection of the profiles at the fracture depth, especially visible in the mean and minimum annual T(z) profile indicates that the fracture locally cools the rock. Mean annual temperature at 2.5-m-depth is even colder than the surface which, as said, is likely warmed by the snow cover. Such a cooling effect may result from air ventilation in the open fracture that has been shown as a important cooling factor of steep rock wall permafrost (Hasler et al. 2011a). Nevertheless, despite this dominant cooling effect, water percolation can occur along the fracture and heat advection could locally warm the rock (Hasler et al. 2011b), but no signal is detected in such sense on the temperature of BH_N. The small inflections visible in BH_E at several depths every year (sect. 6.2) are also possibly induced by bedrock discontinuities, but they have a negligible impact on the overall linear profile which indicates that heat conduction is the dominant heat transfer process (Williams and Smith, 1989). The fracture width is probably the critical factor controlling the magnitude of the perturbation. Thus, the AdM active layer and permafrost temperatures are controlled by different factors interacting each other such as the snow cover and latent heat which delay and dampen short-term responses to climate signal and cooling effect due to air ventilation within open fractures.

7 Conclusion

The high elevation, morphology and accessibility of AdM make it an exceptional site for investigating permafrost of steep rock walls. The available dataset include eight years of rock surface temperature and four years of deep temperatures. The monitoring network of AdM has been designed for investigating the thermal effect of topography, snow cover and fractures on permafrost. The analysis of this new dataset allows for confirmation of previous studies, some of them being empirically proved for the first time:

1. The thermal characteristics of the AdM's rock walls are typical of steep bedrock permafrost. The spatial variability of surface temperature, active layer thickness and timing, and the permafrost thermal regime are mainly controlled by topography.
2. Deep temperature data confirm the characteristics of sub-surface thermal regime predicted by numerical experiments, in particular the coexistence within a single rock peak of warm and cold permafrost, which generates lateral heat fluxes from warm to cold faces.
3. Interannual changes of MAGST are not uniform at all aspects, even in snow free conditions. This may be ascribed to variable cloud formation from year-to-year.
4. Interannual change of snow-covered sensors may be opposite to snow free sensors as the snow can increase the MAGST due to higher thermo-insulation (more precipitations) meanwhile MAGST at snow free sensors can decrease because of reduced solar radiation and lower air temperature.
5. Surface temperature data confirm that a thin (not-insulating) snow cover is able to lower the MAGST because of a strong reduction of surface albedo.
6. Open fractures have a strong, localized cooling effect possibly resulting from air ventilation within the fracture.

Observations from previous studies are extended and new characteristics are highlighted:

7. On south faces, a thick (insulating) snow cover may cool the MAGST because of a prevailing effect of increased surface albedo and latent heat consumption. On north faces, thermo-insulation can dominate and snow can warm MAGST similarly to gentle mountain slopes.

8. The interannual changes of MAGST in snow covered areas are greater on shaded aspects than on sunny faces because the latter combines the controls of solar radiation and snow.

9. The effects of snow cover on ALT in steep rock walls follow the same rules of gentle morphologies. In particular: (i) a thick (insulating) snow cover may reduce cooling during winter leading to a thickening of ALT; (ii) a long-lasting (early summer) snow cover may reduce summer warming leading to a thinning of ALT. Such a contrasting effects may coexist or not both in space (e.g. aspects) and time (e.g. season).

10. Latent heat due to phase change processes of interstitial water in bedrock fractures can dampen active layer and permafrost interannual changes in steep bedrock.

8. Further developments

The AdM thermal characteristics illustrate the complexity of processes controlling the thermal regime of shallow layers in rock wall permafrost that currently challenges model development. Specific investigations addressing the snow control effect may be required to better understand the impact of thick snow accumulations and summer snow falls on ALT and permafrost changes which may contribute in the knowledge development on rock fall activities. The detailed analysis of the pictures showing the evolution of the south and northeast faces, of the snow probes and borehole records at the AdM, will support this project. Investigations on the latent heat consumption in compact bedrock may also be relevant to better understand ALT changes and timing of some snow-covered faces, as well as permafrost evolution over short-time scales. The BH_N fracture constitutes an opportunity to investigate non-conductive heat transfers with adapted method such as a heat conduction scheme. Ground-penetrating radar measurements performed on the northwest face and crossing BH_N borehole offer a clear image of the bedrock discontinuities and constitute additional data for heat flow model development that would integrate the bedrock structure. The combined use of crack-meters, air temperature and boreholes data is promising for developing the understanding of the thermal and mechanical factors in rock wall instabilities.

The here presented data set has been used for statistical and numerical model evaluations designed for mapping the permafrost distribution in the Mont Blanc massif (Magnin et al., 2014) and for predicting the temperature field distribution and evolution over the next century at the AdM (Noetzli et al., 2014b). The statistical model will be used for determining the bedrock temperature and related permafrost thermal regime at the inventoried rock fall locations to analyze the relationship between bedrock temperature and failure.

Acknowledgements: We acknowledge S. Gruber, U. Morra di Cella, E. Cremonese and E. Malet for their participation in installation and data acquisition at the Aiguille du Midi, as well as the *Compagnie des Guides* of Chamonix for their help in the drilling operations, the *Compagnie du Mont Blanc* (especially E. Desvaux) for the access at the site, and Météo France for the air temperature data. We thank A. Hasler and anonymous reviewer for their useful comments and recommendations, and P. Henderson for improving the quality of the English language. This work is supported by the Region Rhône-Alpes (*CIBLE* program).

References

Allen, S. K., Gruber, S., and Owens, I. F.: Exploring steep bedrock permafrost and its relationship with recent slope failures in the Southern Alps of New Zealand, Permafrost Periglac., 20, 345–356, doi:10.1002/ppp.658, 2009.

Boeckli, L., Brenning, A., Gruber, S., Noetzli, J. Permafrost distribution in the European Alps: calculation and evaluation of an index map and summary statistics. The Cryosphere Discuss., 6, 849–891, doi:10.5194/tcd-6-849-2012. 2012.

Cermak, V., Rybach, L. Thermal conductivity and specific heat of minerals and rocks. In Landolt–Börnstein Zahlenwerte and Funktionen aus Naturwissenschaften und Technik, Neue Serie, Physikalische Eigenschaften der Gesteine (V/1a), Angeneister G (ed.). Springer: Berlin; 305–343. 1982.

Deline P.: Recent Brenva rock avalanches (Valley of Aosta): new chapter in an old story? Supplementi di Geografia Fisica e Dinamica Quaternaria, 5, 55–63, 2001.

Deline, P., Alberto, W., Broccolato, M., Hungr, O., Noetzli, J., Ravanel, L., and Tamburini, A.: The December 2008 Crammont rock avalanche, Mont Blanc massif area, Italy, Nat. Hazard Earth Sys., 11, 3307–3318, 2011.

Deline, P., Gardent, M., Magnin F., and Ravanel, L.: The morphodynamics of the Mont Blanc massif in a changing cryosphere: a comprehensive review, Geogr. Ann. A, 94(2), 265–283, 2012.

Fischer, L., Kääb, A., Huggel, C., and Noetzli, J.: Geology, glacier changes, permafrost and related slope instabilities in a high-mountain rock wall: Monte Rosa east face, Italian Alps, Nat. Hazard Earth Sys., 6, 761–772, 2006.

Gruber, S., and Haeberli, W.: Permafrost in steep bedrock slopes and its temperature related destabilization following climate change, J. Geophys. Res., 112, F02S13, doi:10.1029/2006JF000547, 2007.

Gruber S., Haeberli W.: Mountain permafrost. *In*: Margesin R. (Ed.). Permafrost soils. Biology series, Springer, 16: 33-44, 2009.

Gruber, S., Peter, M., Hoelzle, M. Woodhatch, I., and Haeberli. W.: Surface temperatures in steep alpine rock faces: a strategy for regional-scale measurement and modelling, In: L. Arenson (Editor), 8th International Conference on Permafrost, Proceedings. Swets & Zeitlinger, Lisse, Zürich, pp. 325-330, 2003.

Gruber, S., Hoelzle, M., and Haeberli, W.: Permafrost thaw and destabilization of Alpine rock walls in the hot summer of 2003, Geophys. Res. Lett., 31, L13504, doi:10.1029/2004GL0250051, 2004a.

Gruber, S., Hoelzle, M., and Haeberli, W.: Rock-wall temperatures in the Alps: modelling their topographic distribution and regional differences, Permafrost Periglac., 15, 299–307, doi: 10.1002/ppp.501, 2004b.

Gubler, S., Fiddes, J., Keller, M., Gruber, S.: Scale-dependent measurement and analysis of ground surface temperature variability in alpine terrain, The Cryosphere, 5, 431–443, 2011.

Hanson, S. and Hoelzle, M. The thermal regime of the active layer at the Murtèl rock glacier based on data from 2002. Permafrost Periglac., 15: 273–282. doi: 10.1002/ppp.499. 2004.

Harris, S., and A. Corte (1992), Interactions and relations between mountain permafrost, glaciers,snow and water, Permafrost Periglac., 3(2), 103–110.

Hasler, A., Gruber, S., and Haeberli, W.: Temperature variability and offset in steep alpine rock and ice faces, The Cryosphere, 5, 977–988, doi:10.5194/tc-5-977-2011, 2011a.

Hasler, A. Gruber, S. Font, M. Dubois, A. Advective heat transport in frozen rock clefts - conceptual model, laboratory experiments and numerical simulation. Permafrost Periglac., 22, 378–349, doi: 10.1002/ppp.737, 2011b.

Hipp, T., Etzelmüller, B. and Westermann, S. Permafrost in Alpine Rock Faces from Jotunheimen and Hurrungane, Southern Norway. Permafrost Periglac., 25: 1–13. doi: 10.1002/ppp.1799, 2014.

Hoelzle, M., Wegmann, M. and Krummenacher, B.: Miniature temperature dataloggers for mapping and monitoring of permafrost in high mountain areas: first experience from the Swiss Alps. Permafrost Periglac., 10: 113–124. doi: 10.1002/(SICI)1099-1530(199904/06)10:2<113::AID-PPP317>3.0.CO;2-A, 1999.

Huggel, C., Caplan-Auerbach, J., and Wessels, R.: Recent extreme avalanches triggered by climate change, EOS, Transactions American Geophysical Union, 89: 469–470, 2008.

Huggel, C., Zgraggen-Oswald, S., Haeberli, W., Kääb, A., Polkvoj, A., Galushkin, I., and Evans, S.G.: The 2002 rock/ice avalanche at Kolka/Karmadon, Russian Caucasus: assessment of extraordinary avalanche formation and mobility, and application of Quick- Bird satellite imagery, Nat. Hazard Earth Sys., 5, 173–187, doi:10.5194/nhess-5-173-2005, 2005.

Krautblatter, M., Huggel, C., Deline, P., and Hasler, A. Research Perspectives on Unstable High-alpine Bedrock Permafrost: Measurement, Modelling and Process Understanding. Permafrost Periglac., 23: 80–88, DOI: 10.1002/ppp.740 2011.

Juliussen, H. and Humlum, O. Towards a TTOP ground temperature model for mountainous terrain in central-eastern Norway. Permafrost Periglac., 18: 161–184. doi: 10.1002/ppp.586, 2007.

Kukkonen, I. T., and J. Safanda. Numerical modelling of permafrost in bedrock in northern Fennoscandia during the Holocene, Global Planet. Change, 29, 259– 273, 2001.

Leloup, P. H., Arnaud, N., Sobel, E. R. and Lacassin, R.: Alpine thermal and structural evolution of the highest external crystalline massif: The Mont Blanc. Tectonics, 24, TC4002, doi: 10.1029/2004TC001676, 2005.

Le Roy, M.: Reconstitution des fluctuations glaciaires holocènes dans les Alpes occidentales, Thèse de Doctorat de Géographie, Université de Savoie, Le Bourget du Lac, 344 pp, 2012.

Luetschg, M., Lehning, M., and Haeberli, W.: A sensitivity study of factors influencing warm/thin permafrost in the Swiss Alps, J. Glaciol., 54, 696–704, 2008.

Magnin, F., Brenning, A., Bodin, X., Deline, P., Ravanel, L. Manuscript submitted. Statistical modelling of rock wall permafrost distribution: application to the Mont Blanc massif. Géomorphologie

Noetzli, J., Gruber, S., Kohl, T., Salzmann, N., and Haeberli, W.: Three-dimensional distribution and evolution of permafrost temperatures in idealized high-mountain topography, J. Geophys. Res-Earth, 112(F2), F02S13, doi:10.1029/2006JF000545, 2007.

Noetzli, J., Christiansen, H. H., Guglielmin, M., Romanovsky, V. E., Shiklomanov, N. I., Smith, A.L. and Zhao, L.: [Global climate] Permafrost thermal state [in “State of the Climate in 2013”]. *Bull. Amer. Meteor. Soc.*, **95** (7), S15–S16, 2014a.

Noetzli, J., Ravanel L., and Deline P. in prep. Combining measurements and modelling to describe the permafrost conditions at the Aiguille du Midi (3842 m asl, Mont Blanc Massif). The Cryosphere.

PERMOS: Permafrost in Switzerland 2002/2003 and 2003/2004, in: Vonder Mühll, D. (eds.), Glaciological Report (Permafrost) No. 4/5 of the Cryospheric Commission of the Swiss Academy of Sciences, Zürich, 121 pp, 2007.

PERMOS: Permafrost in Switzerland 2008/2009 and 2009/2010, in: Noetzli, J. (eds.), Glaciological Report (Permafrost) No. 10/11 of the Cryospheric Commission of the Swiss Academy of Sciences, Zürich, 95 pp, 2013.

Pogliotti, P.: Influence of Snow Cover on MAGST over Complex Morphologies in Mountain Permafrost Regions. PhD thesis, Turin, Italy, Università degli Studi di Torino. 79 pp, 2011.

Pogliotti, P., Cremonese, E., M. di Cella, U., Gruber, S., and Giardino M. Thermal diffusivity variability in alpine permafrost rock walls, in Proceedings of Ninth International Conference on Permafrost, Fairbanks, Institute of Northern Engineering, University of Alaska, vol. 2, pp. 1427–1432, 2008.

Ravanel, L. and Deline P.: Climate influence on rockfalls in high-Alpine steep rock walls: the north side of the Aiguilles de Chamonix (Mont Blanc massif) since the end of the 'Little Ice Age', The Holocene, 21, 357–365, doi: 10.1177/0959683610374887, 2010.

Ravanel, L., Allignol, F., Deline, P., Gruber, S., and Ravello, M.: Rock falls in the Mont Blanc Massif in 2007 and 2008, Landslides, 7, 493–501, 2010.

Ravanel, L., Deline, P., Lambiel, C., and Vincent C.: Intability of a high Alpine rock ridge: the lower Arête des Cosmiques, Mont Blanc massif, France, Geogr. Ann. A, 95, 51–66, doi: 10.1111/geoa.12000, 2012.

Romanovsky, V. E., Smith, S. L., Christiansen, H. H., Shiklomanov, N. I., Streletskiy, G. A., Drozdov, D. S., Malkova, G. V., Oberman, N. G., Kholodov, A. L., Marchenko, S. S.: [Global climate] Terrestrial permafrost [in "State of the Climate in 2013"]. *Bull. Amer. Meteor. Soc.*, **95** (7), S139–S141, 2014.

Smith, M. W. and Riseborough, D. W. Permafrost monitoring and detection of climate change. Permafrost Periglac., 7: 301–309. doi: 10.1002/(SICI)1099-1530(199610)7:4<301::AID-PPP231>3.0.CO;2-R, 1996.

Smith, M. W. and Riseborough, D. W. Climate and the limits of permafrost: a zonal analysis. Permafrost Periglac., 13: 1–15. doi: 10.1002/ppp.410, 2002.

Williams, P. J. and Smith, M. W.: The frozen earth, 1 ed., Studies in polar research, Cambridge University Press, Cambridge, 306 pp., 1989.

Tables

Site Code	Elevation [m a.s.l]	Aspect [°]	Slope [°]	Sensor depths [m]	Estimated snow accumulation [m]
BH_S	3753	135	55	0.14, 0.34, 0.74, 1.04, 1.34, 1.64, 2.14, 2.64, 3.64, 4.64, 6.64, 8.64, 9.64	> 0.8
BH_N	3738	345	90	0.3, 0.5, 0.7, 0.9, 1.1, 1.4, 1.7, 2, 2.5, 3, 4, 5, 7, 9, 10	> 1.0
BH_E	3745	50	65	0.3, 0.5, 0.7, 0.9, 1.1, 1.4, 1.7, 2, 2.5, 3, 4, 5, 7, 9, 10	< 0.6
W1	3825	270	80	0.1	0
S1	3820	140	74	0.1	0
N1	3820	354	84	0.1	0
E1	3823	124	60	0.1	0
N2	3820	334	80	0.03, 0.1, 0.3, 0.55	0
E2	3820	118	60	0.03, 0.1, 0.3, 0.55	0
S2	3815	160	85	0.03, 0.1, 0.3, 0.55	0
W2	3825	270	85	0.03, 0.1, 0.3, 0.55	0
S3	3820	158	70	0.03, 0.1, 0.3, 0.55	0.5 to 1.0
AT	3845	0	0		0

Table 1. Instrument positions.

BH: borehole thermistor chains, x1 and x2: rock surface temperature loggers, AT: air temperature. Estimated snow accumulation: from automatic cameras and probes for BH_S and BH_E (winter 2011 and 2012), from field observation for S3 and BH_N.

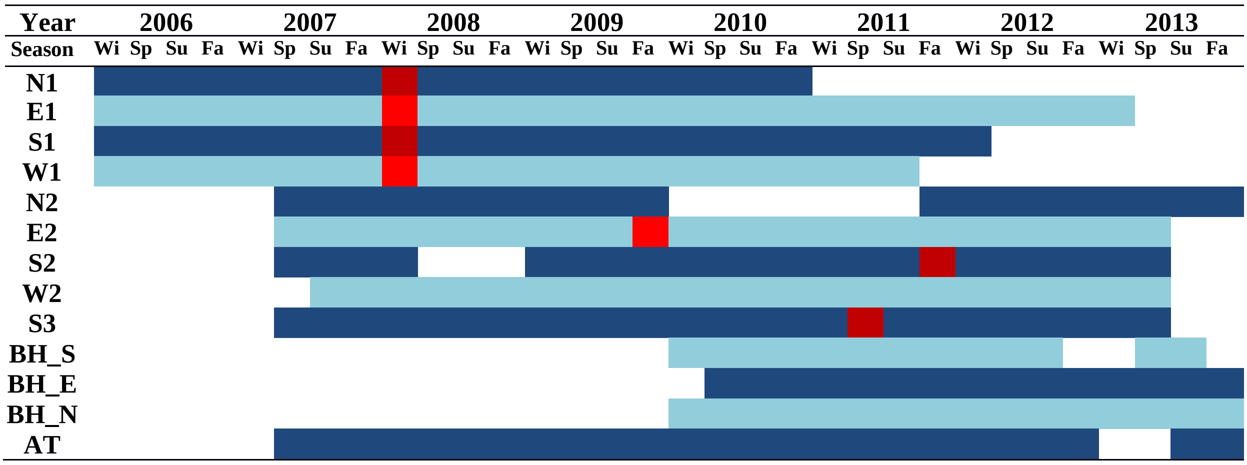

Table 2. Data availability after gap filling.

Wi: December, January, February; **S**p: March, April, May; **Su**: June, July, August; **Fa**: September, October, November.

Red sections indicate where gaps <1.5 month per year have been filled in order to calculate annual means but seasonal means were not calculated for the seasons in question. The time series interrupted with white gap areas indicate that annual mean is not computed for the concerned year.

Year	BH_E			BH_S			BH_N			MAAT
	ALT [m]	**Max. ALT [dd.mm]**	**$MART_{10m}$ [°C]**	**ALT [m]**	**Max. ALT [dd.mm]**	**$MART_{10m}$ [°C]**	**ALT [m]**	**Max. ALT [dd.mm]**	**$MART_{10m}$ [°C]**	
2010	3.1	27.07	-	5.2	23.10	-1.4	1.8	28.08	-4.7	-9
2011	2.7	30.08	-3.8	5.9	22.10	-1.5	2.3	18.09	-4.6	-6.7
2012	3.3	26.08	-3.6	-	-	-	2.5	26.08	-4.3	-7.7
2013	3.4	08.09	-3.6	5.8	30.09	-	2.2	25.08	-4.5	-

Table 3. Borehole and air temperature records.

ALT: Active Layer Thickness

$MART_{10m}$: Mean Annual Rock Temperature at 10 m deep

Figures

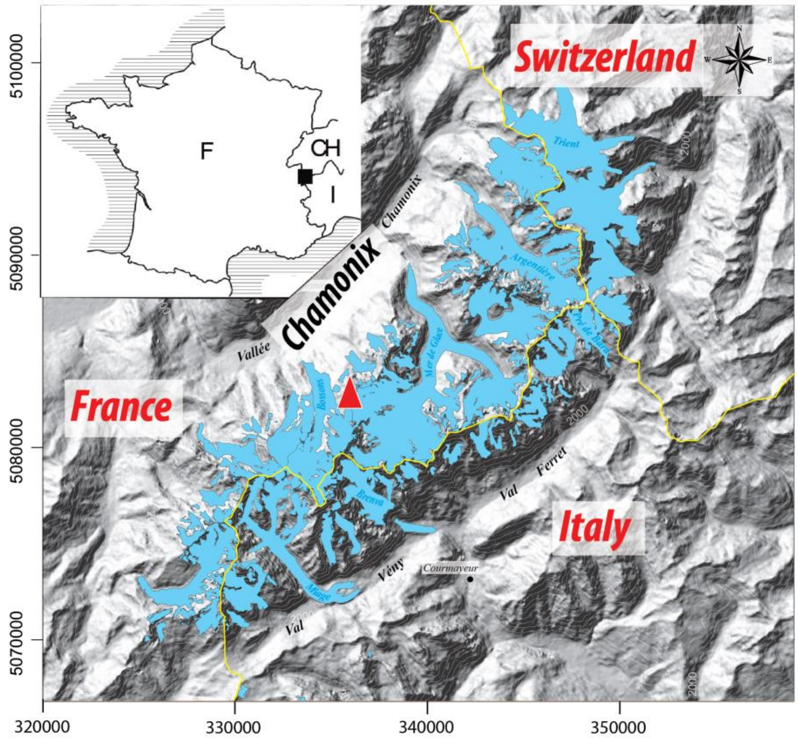

Figure 1. Location of the Mont Blanc Massif and the Aiguille du Midi (red triangle) (modified from Le Roy, 2012).

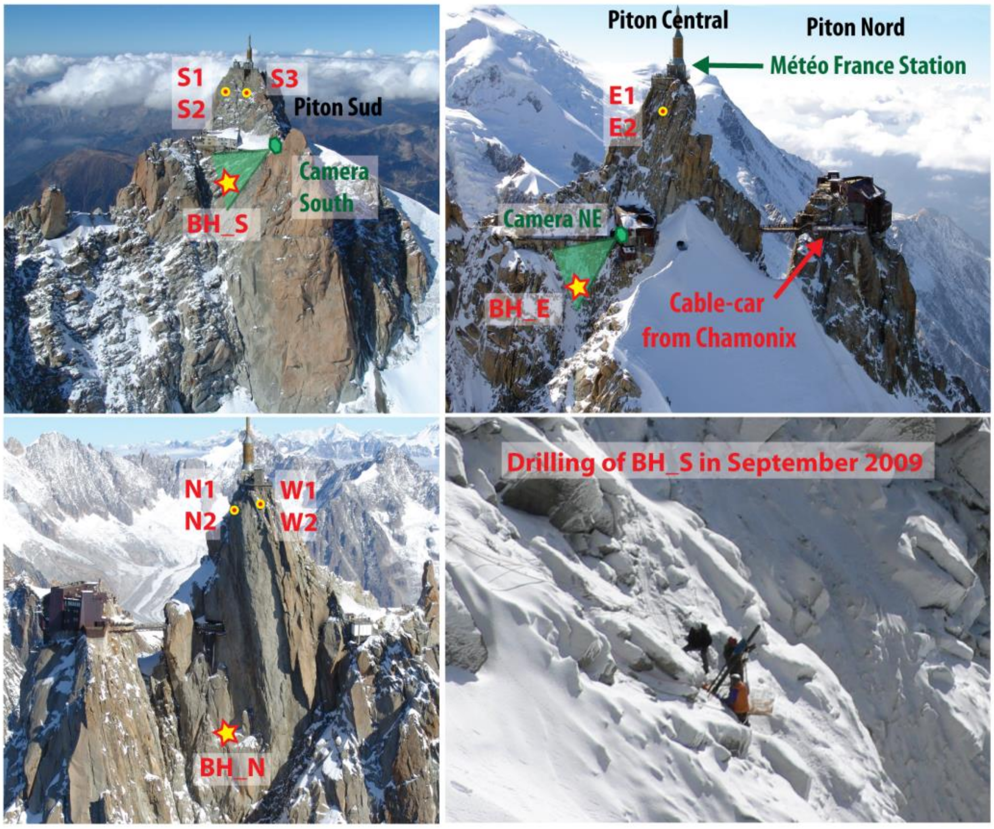

Figure 2. The Aiguille du Midi with camera, RST, and BH logger locations.
Pictures: S. Gruber (top left and right, bottom left); P. Deline (bottom right).

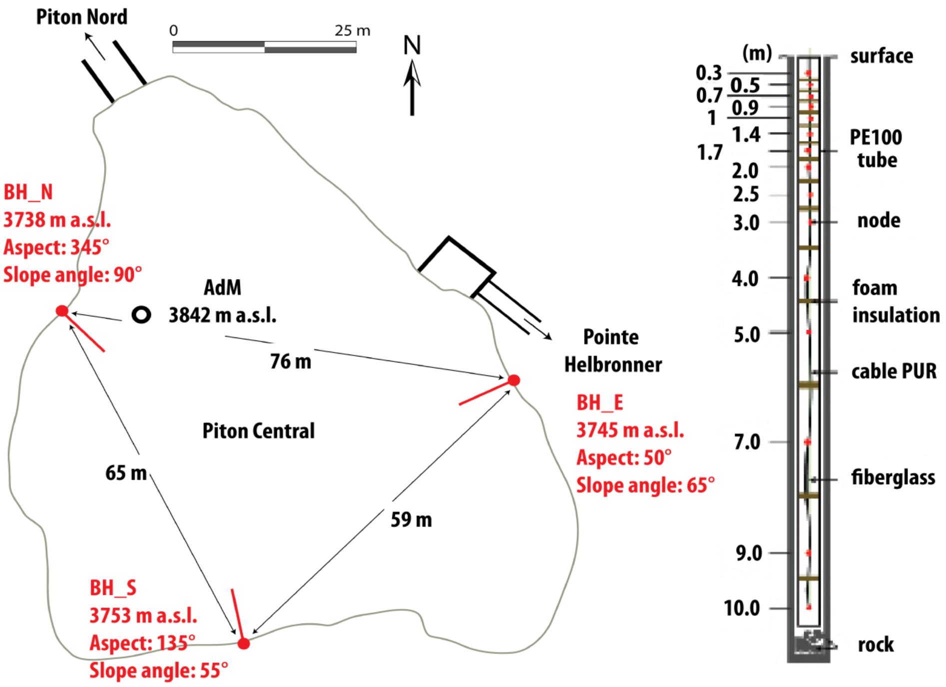

Figure 3. Borehole positions and components.

Left: Horizontal cross-section through the AdM's Piton Central. Borehole positions are marked in red.

Right: 10-m-long, 15-node thermistor chain installed in the boreholes.

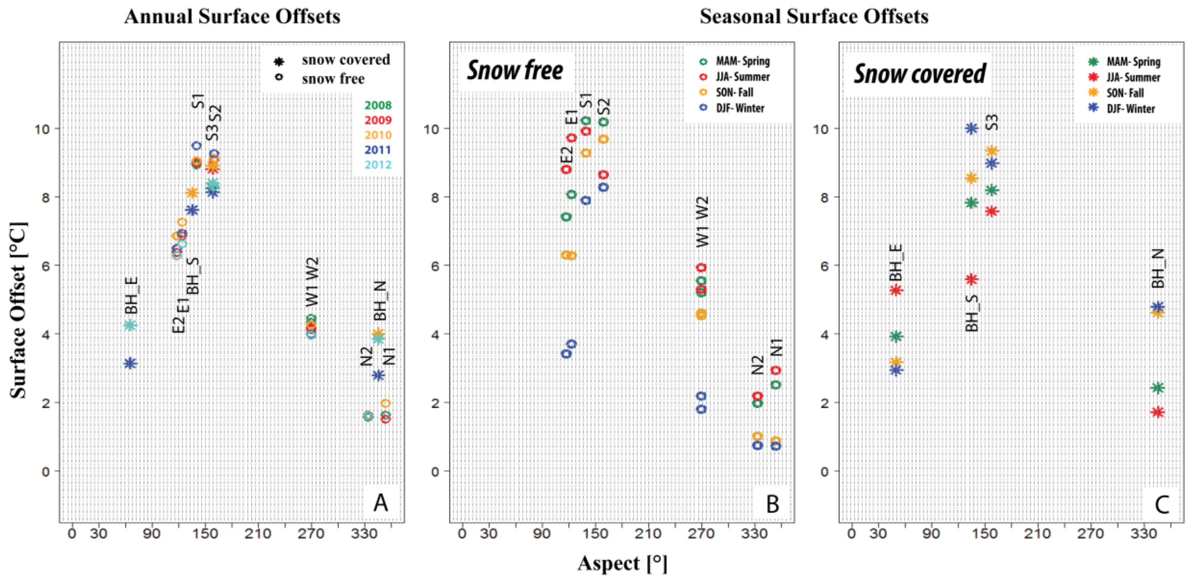

Figure 4. Annual and Seasonal Surface Offsets calculated from sensors at 0.3 m deep.

ASOs are shown for all the available years. SSOs are the mean values for the available seasons for each logger listed in Table 2.

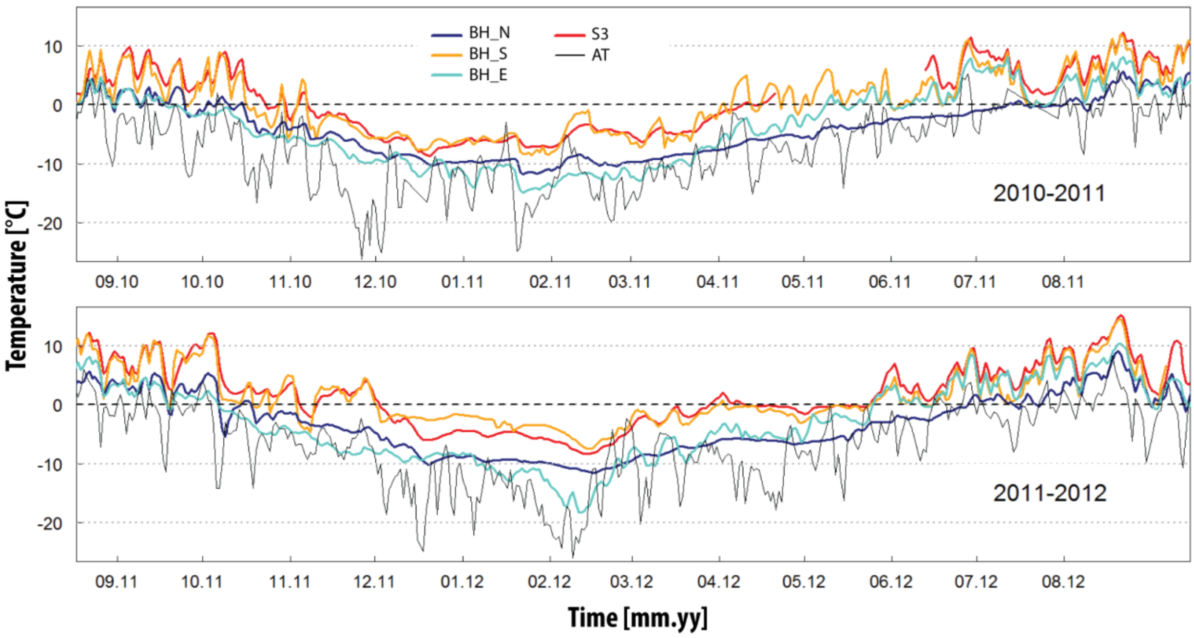

Figure 5. Daily temperature records at 0.3 m deep for snow-covered sensors for the 2010-2011 and 2011-2012 hydrological years.

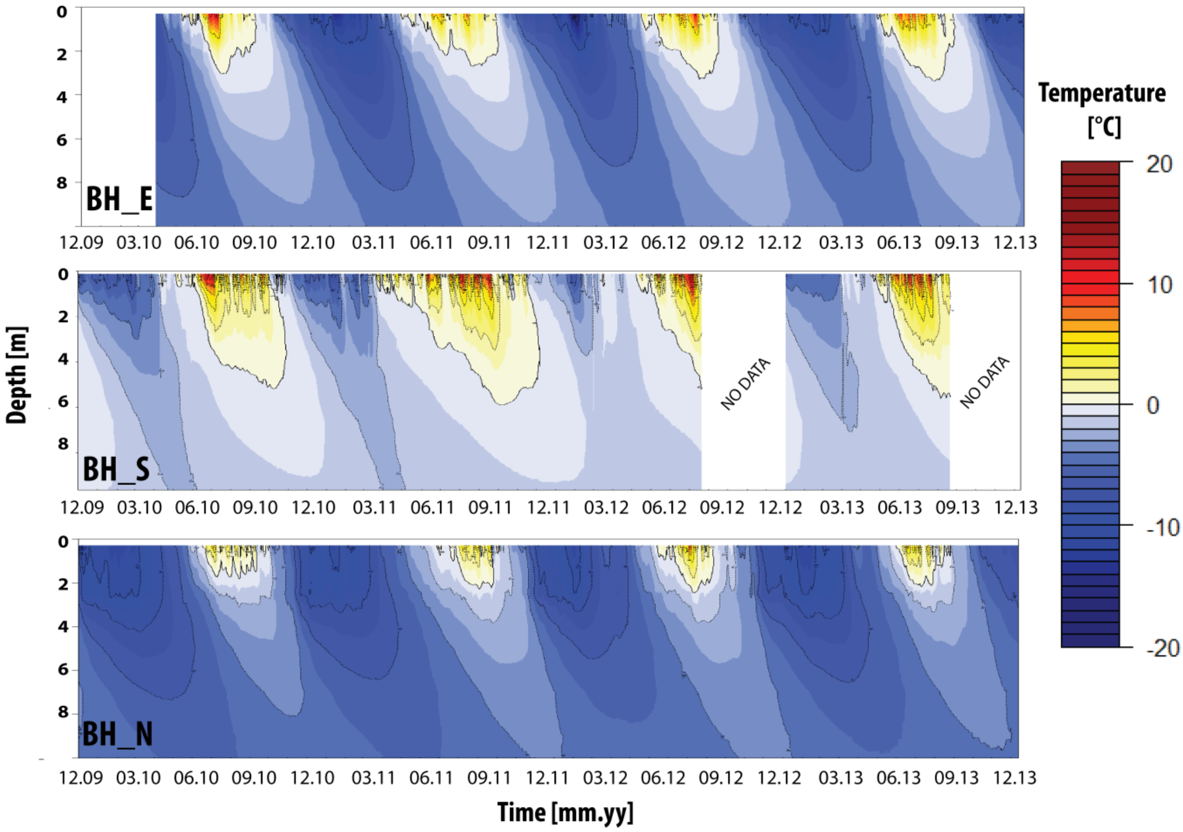

Figure 6. Daily temperature records in the AdM boreholes from December 2009 to January 2014.

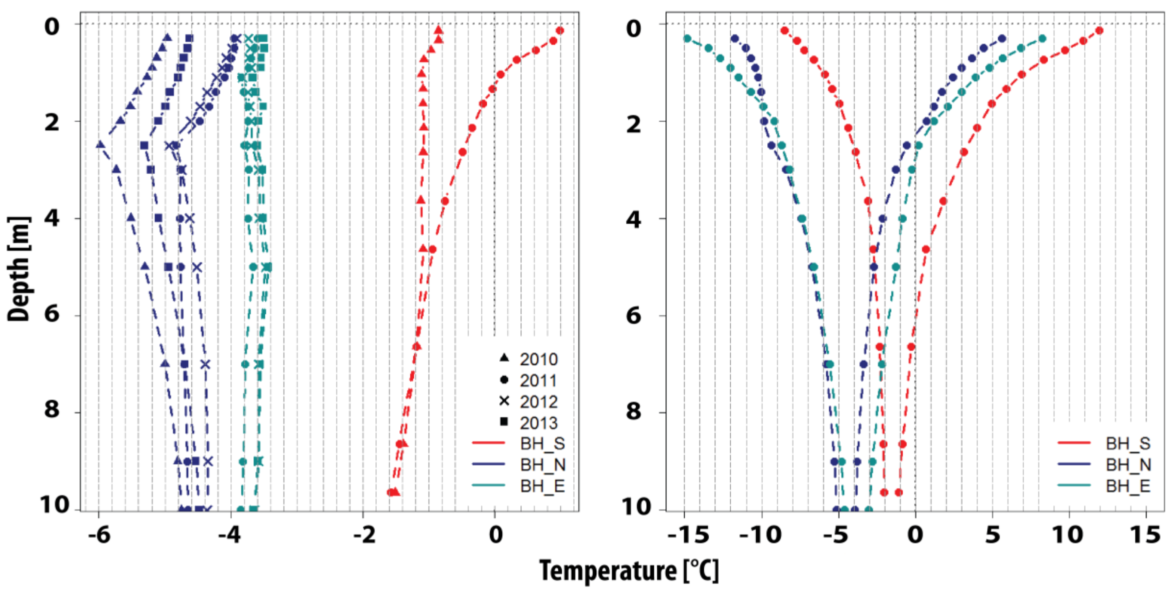

Figure 7. Mean T(z) profiles (A) and 2011 temperature envelopes (B) of the AdM boreholes.